Modal Analysis of a DFIG-Based Wind Farm Interfaced with a Series Compensated Network

Lingling Fan, *Senior Member, IEEE*,Chanxia Zhu, *Student Member, IEEE*, Zhixin Miao, *Senior Member, IEEE*, Minqiang Hu

***Abstract*—Interests of subsynchronous resonance (SSR) in series compensated electric networks with wind power penetration have arisen recently. To better understand the nature of such systems, modal analysis of a doubly-fed induction generator (DFIG)-based wind energy system interconnected with a series compensated electric network is conducted in this paper. The system model is built in Matlab/Simulink. The major contributions of the paper include: (i) identification of the four system modes (SSR, supersynchronous, electromechanical and shaft modes) of a DFIG-based wind farm interfaced with a series compensated network, (ii) investigation of the impacts of various parameters and operating conditions on those modes and (iii) prediction of the dynamic performance of the system using modal analysis and confirmation of such prediction via time-domain simulation results.**

***Index Terms*—DFIG, SSR, Participation Factor, Modal Analysis, Eigenvalues**

I. Introduction

SUBSYNCHRONOUS resonance (SSR) phenomenon happened in series compensated transmission networks and caused extensive damage to turbine-generator shafts in power plants in history [1]. It is of great interest to the utility industry. With the increasing penetration of wind power in transmission networks, interests of SSR phenomenon in wind energy systems have arisen. In regions where series compensated long distance transmission networks are used and abundant wind power sources are available, the interaction of wind power and the network LC resonance modes is especially of high interest. Several recent research papers have addressed SSR issues in wind farms interconnected with series compensated networks [2]–[4].

Reference [2] discusses SSR phenomena of a self-excited double induction generator based wind farm interconnected with a series-compensated network. Impacts of wind speeds and compensation levels on SSR are investigated. FACTS devices such as TCSC and SVC are used to demonstrate how to mitigate SSR in such systems. Reference [3] investigates the small signal stability issues of a DFIG-based wind farms interconnected with a series compensated network. Though the word "SSR" is not mentioned in the paper, the dominant mode is the electric network SSR mode. Compared with the wind farm in [2], the DFIG-based wind farm in [3] is equipped with back to back converters and has control capabilities. Therefore, besides wind speeds and compensation levels, impacts of the parameters of the current control loops of the converters on small signal stability are investigated. In [4], the focus is on control design and testing using STATCOM to mitigate SSR in a wind energy system similar as that in [2].

A thorough small signal analysis or modal analysis of series compensated networks with wind power penetration can improve the understanding of such systems and facilitate SSR mitigation. As DFIG is the state-of-the-art wind generator technology, DFIG-based wind energy systems should be the focus of such investigation. Though Reference [3] presents a small signal analysis of a DFIG-based wind farm interconnected with a series compensated network, only the SSR mode is identified as the dominant mode and further studies. All other system modes are not presented. Furthermore, the shaft system is modeled as one-mass system and hence the shaft mode of the wind turbine cannot be observed. Small signal analysis of DFIG-based wind energy systems has also been performed in [5] and [6] with the shaft mode captured. However, the network dynamics are ignored in the models and SSR phenomena cannot be captured. In addition, a constant turbine power is assumed and only one wind speed is discussed in [5] and [6].

The presentation of an overview picture of the system modes under a changing operating condition (*e.g.*, the varying wind speeds) is the purpose of this paper. Small signal analysis or modal analysis will be performed to identify the system modes and their characteristics. Also, time responses of the electrical and mechanical system variables such as voltages, currents, speeds and torques will be predicted using modal analysis and confirmed by nonlinear time-domain simulations in Matlab/Simulink. This study will lay the foundation for future works in SSR mitigation and stability enhancement in systems with wind penetration.

The rest of the paper is organized as follows. Section II describes the study system and the models of such system. Section III presents modal analysis, participation factors, and time response coefficients. Identification of the system modes is presented in Section IV using eigenvalue analysis and participation factors. Section V presents the time response coefficients of the study system and the nonlinear time-domain simulation results. The relationship between the time response coefficients and the dynamic responses in simulation results is explained. Section VI concludes the paper.

II. Study System

The study system is shown in Fig. 1 where a DFIG-based wind farm (100 MW from aggregation of 2 MW units)

L. Fan and Z. Miao are with Department of Electrical Engineering, University of South Florida, Tampa, FL 33620. C. Zhu and M. Hu are with Southeast University. Email: linglingfan@usf.edu. Phone: (813)974-2031.

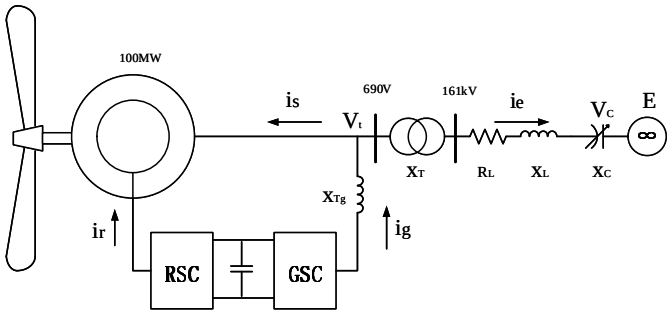

Fig. 1. The system structure.

is connected to a series-compensated line whose parameters correspond to the IEEE first benchmark model for SSR studies [7]. The wind farms can be considered as coherent generators and can be represented by one large DFIG. This approach has been practiced in system studies [8]. The parameters of a single 2MW DFIG and the equivalent DFIG are listed in Appendix Table IX. The parameters of the network are listed in Appendix Table X.

The study system consists of an equivalent DFIG, its back to back rotor side converter (RSC) and grid-side converter (GSC), the drive train and the transmission line. A 6th order model is used to describe the dynamics of the stator and rotor currents of an induction generator in the synchronous reference frame [9]. A two-mass model is used to describe the dynamics of the rotor and the drive train [5]. The parameters of the shaft are given in Appendix Table XI. The high switching dynamics at the order of kilo Hz of the IGBT-based converter are ignored in the modeling process while both the inner and outer control loops of the RSC and GSC are taken into consideration. The dynamics of the capacitor in the dc-link between the RSC and the GSC is modeled as a first-order differential equation.

Unlike models for transient stability where the dynamics of the electric network are ignored, in this study, to demonstrate the electric network LC resonance mode, the dynamics of the current through the inductor and the dynamics of the voltage across the series-connected capacitor are modeled in differential equations. Further, since the wind farm is modeled in the synchronous reference frame, the transmission network should also be modeled in the same reference frame for simulations and small signal analysis [10]. The details of the models and the modeling procedure can be found in [11] and [12].

In this study, the RSC and GSC control loops are modeled, where the inner loops are current control loops and the outer loops are the power/voltage control loops. For the RSC control loops, the qd-axis loops are to track the active and reactive power references respectively. Maximum power point tracking is used to determine the active power order of the q-axis control. For the GSC control loops, the qd-axis loops are to track the dc-link reference voltage and the wind farm terminal voltage respectively. The detailed description of the GSC control scheme can be found in [13] and and the detailed description of the control schemes of both converters can be found in [12].

III. Modal Analysis, Participation Factors, and Time Response Coefficients

Modal analysis or small signal analysis has been popularly used in power system stability analysis. The application areas include low frequency oscillation stability [14] and SSR stability [15]. In [16], modal analysis and its applications in both areas are covered. More recently, high bandwidth (six-sample per cycle) model is used in accurate eigenvalue analysis of SSR performance of TCSC control schemes [17].

Modal analysis is a technique based on modal decomposition. The mathematical model of the linearized study system can be written as a set of differential algebraic equations given by:

$$\begin{cases} \dot{X} = AX + BU \\ Y = CX + DU \end{cases} \tag{1}$$

where X is the state variable vector, Y is the output vector, U is the input vector, A is the state matrix of size $n \times n$, B is the input matrix of size $n \times r$, C matrix has a size of $m \times n$ and D is the matrix which defines the proportion of input which appears directly in the output ($m \times r$).

(1) can be transformed into a set of decoupled dynamic equations by introducing a new state vector $\widetilde{X}$, where $\widetilde{X} = WX$ and W is the left eigenvector matrix. Its inverse is the right eigenvector matrix and is denoted as V. W, V and the state matrix A have the following relationship:

$$WAV = \Lambda = \begin{bmatrix} \lambda_1 & & & \\ & \lambda_2 & & \\ & & \ddots & \\ & & & \lambda_n \end{bmatrix} \tag{2}$$

The new set of differential and algebraic equations can be written as:

$$\begin{cases} \dot{\widetilde{X}} = \Lambda \widetilde{X} + WBU \\ Y = CV\widetilde{X} + DU \end{cases} \tag{3}$$

Since Λ is a diagonal matrix, the dynamics of each new state variable $\widetilde{X_i}$ is now decoupled, *i.e.*, it is determined by its own initial condition, the input and the i-th system mode λ_i but not related to other state variables $\widetilde{X_j}$ ($j \neq i$).

A. Participation Factor

Participation factor is used to measure the effect of X_i on the k-th mode. The definition of participation factors for an eigenvalue is given as:

$$p_{ki} = \frac{|V_{ik}||W_{ki}|}{\sum_{k=1}^{n} |V_{ik}|\,|W_{ki}|} \tag{4}$$

p_{ki} denotes the impact of the i-th state variable on the k-th eigenvalue. Participation factor can be computed from the eigenvector matrices (V and W).

TABLE I
SYSTEM MODES AT DIFFERENT WIND SPEEDS WITH 75% COMPENSATION LEVEL

	Mode 1: $\lambda_{1,2}$ (Hz)	Mode 2: $\lambda_{3,4}$ (Hz)	Mode 3: $\lambda_{5,6}$ (Hz)	Mode 4: $\lambda_{7,8}$ (Hz)
7 m/s	4.9$\pm j$123.2 (19.6)	-10.4$\pm j$629 (100)	-12.7$\pm j$99.1(15.8)	-1$\pm j$5.8(0.92)
8 m/s	-2.1$\pm j$121.8 (19.4)	-10$\pm j$629.1(100)	-5.7$\pm j$ 63.2(10.1)	-1.5$\pm j$5.4(0.86)
9 m/s	-4.3$\pm j$121.4 (19.3)	-9.6$\pm j$629.2(100)	-2.5$\pm j$30.5 (4.85)	-1.4 $\pm j$2.8 (0.45)
10 m/s	-5.4$\pm j$120.7 (19.2)	-9.3$\pm j$629.4 (100)	-5.9 $\pm j$27.8(4.42)	0.5 $\pm j$4.4 (0.70)

TABLE II
SYSTEM MODES AT 7M/S WIND SPEED WITH DIFFERENT COMPENSATION LEVELS

	Mode 1: $\lambda_{1,2}$ (Hz)	Mode 2: $\lambda_{3,4}$ (Hz)	Mode 3: $\lambda_{5,6}$ (Hz)	Mode 4: $\lambda_{7,8}$ (Hz)
25%	-4.4$\pm j$230.6 (36.7)	-7.7$\pm j$522.6 (83.2)	-3.5$\pm j$97.1 (15.5)	-0.9$\pm j$6 (0.95)
50%	-2.6$\pm j$169.6 (27.0)	-9 $\pm j$582.2 (92.7)	-5.2$\pm j$98 (15.6)	-0.9$\pm j$5.9 (0.94)
75%	4.9$\pm j$123.2 (19.6)	-10.4$\pm j$629 (100)	-12.7$\pm j$99.1(15.8)	-1$\pm j$5.8(0.92)
95%	12$\pm j$105.2 (16.7)	-11.4 $\pm j$660.5 (105)	-19.9$\pm j$86.8 (13.8)	-1.1 $\pm j$5.7 (0.91)

B. Time Response Coefficients

Assume that the linear system under discussion has no inputs, then from (3), the decoupled first order equation which describes the dynamics of $\widetilde{X_i}$ is given by:

$$\dot{\widetilde{X_i}} = \lambda_i \widetilde{X_i}. \tag{5}$$

The time-domain response can be given by:

$$\widetilde{X}_i(t) = e^{\lambda_i t}\widetilde{X}_i(0) \tag{6}$$

where $\widetilde{X}_i(0)$ is the initial value of $\widetilde{X}_i$ and $\widetilde{X}_i(0) = WX_i(0)$.

Therefore the time response of the original state vector is given by:

$$\begin{aligned} X_i(t) &= \sum_{k=1}^{n} V_{ik}\widetilde{X}_k(t) \\ &= \sum_{k=1}^{n} V_{ik}e^{\lambda_k t}\widetilde{X}_k(0) \\ &= \sum_{k=1}^{n} V_{ik}e^{\lambda_k t}\left[\sum_{j=1}^{n} W_{kj}X_j(0)\right] \end{aligned} \tag{7}$$

In another word, the time response of the component in $X_i(t)$ which corresponds to eigenvalue λ_k can be written as:

$$\begin{aligned} X_i^k(t) &= C_i^k e^{\lambda_k t} \\ \text{where } C_i^k &= \sum_{j=1}^{n} V_{ik}W_{kj}X_j(0) \end{aligned} \tag{8}$$

Thus, the time response coefficients C_i^k can be determined by the eigenvector matrices (V and W) and the initial conditions of the state variables.

IV. SYSTEM MODES IDENTIFICATION

In this paper, maximum power point tracking is modeled. For each wind speed, the wind turbine's rotating speed will have a corresponding optimum value. The following table gives the relationship of the wind speed, the rotating speed and the torque.

Eigenvalue analysis of the study system at 75% compensation level at different wind speeds are conducted with four oscillatory system modes shown in Table I. These four system modes at different compensation levels are shown in Table II.

TABLE III
WIND SPEED, ROTOR SHAFT SPEED AND MECHANICAL POWER LOOKUP TABLE.

v_{wind}	7 m/s	8 m/s	9 m/s	10 m/s	11 m/s	12 m/s
ω_m	0.75	0.85	0.95	1.05	1.15	1.25
P_m	0.32	0.49	0.69	0.95	1.25	1.60
$T_m = \frac{P_m}{\omega_m}$	0.43	0.58	0.73	0.90	1.09	1.28

The first task is to identify the nature of the four modes. From the frequency range, $\lambda_{1,2}$ could be the SSR mode while $\lambda_{3,4}$ represent the super-synchronous mode. $\lambda_{7,8}$ could be the shaft mode and $\lambda_{5,6}$ are difficult to identify.

A. Identification of SSR mode and supersynchronous mode

The frequency of the electric network resonance mode f_n is given by [15]:

$$f_n = f_e\sqrt{\frac{X_c}{X_L}} \tag{9}$$

where X_L is the total inductive reactance, X_c is the total capacitive reactance and f_e is the nominal system frequency. This network oscillatory mode with a frequency of f_n in stators will have a corresponding component induced in rotor circuits with a frequency of $(\pm f_n - f_m)$ (f_m is the frequency corresponding to the rotating speed). Interactions of the stator currents and the rotor currents lead to the electromagnetic torque. Hence in the electromagnetic torque, besides the dc component, there will be two components, one with a frequency of $(60 - f_n)$ (complementary of the SSR network mode) and the other with a frequency of $(60 + f_n)$ for the supersynchronous mode. In this study, the models are built in a synchronous reference frame. Hence the network mode reflected in a stationary circuit with a frequency of f_n has a frequency of $(60 - f_n)$ when the stationary circuits are observed from the synchronous rotating reference frame. The supersynchronous mode is reflected in the electromagnetic torque which is not a circuit variable. Hence in the synchronous rotating reference frame, this mode will be observed to have a frequency of $(60 + f_n)$.

At 75% compensation level, an estimation of the electric network resonance mode based on (9) can be performed where X_c is the reactance of the series compensation and X_L is the total inductive reactance of the system. In this

TABLE IV
PARTICIPATION FACTOR AT DIFFERENT COMPENSATION LEVEL WITH 7M/S WIND SPEED

State Variable	25% compensation level		50% compensation level		95% compensation level	
	SSR mode -4.4+j230.6	shaft mode -0.9+j6	SSR mode -2.6+j169.6	shaft mode -0.9+j5.9	SSR mode 12+j105.2	shaft mode -1.1±j5.7
q−axis stator current i_{qs}	0.2304	0.0021	0.2391	0.0032	0.3376	0.0082
d−axis stator current i_{ds}	0.2322	0.0607	0.2387	0.0809	0.0448	0.1501
q−axis rotor current i_{qr}	0.2254	0.0025	0.2368	0.0036	0.3471	0.0087
d−axis rotor current i_{dr}	0.2269	0.0728	0.2360	0.0945	0.0444	0.1667
q−axis line current i_{qe}	0.0186	0	0.0107	0	0.0013	0.0001
d−axis line current i_{de}	0.0182	0.0031	0.0104	0.0043	0.009	0.0082
turbine speed ω_t	0	0.0773	0	0.0742	0	0.0636
machine speed ω_m	0.0001	**0.3414**	0.0003	**0.3202**	0.0026	**0.2468**
Torque in mass 1−2 T_{12}	0	**0.4353**	0	**0.4143**	0	**0.3405**
q−axis capacitor voltage v_{qc}	0.0237	0.0006	0.0135	0.0017	0.0066	0.0061
d−axis capacitor voltage v_{dc}	0.0239	0	0.0137	0	0.0013	0.0002

study X_c is 75% of the line reactance X_{line} while the total inductive reactance X_L should include the line reactance, the transformer reactance and the machine circuit reactance. An estimation finds that f_n is about 42 Hz for 75% compensation level. Since the synchronous reference frame is used to model the system, this mode reflecting in stationary circuits now becomes 18 Hz in the model. $\lambda_{1,2}$ has a frequency close to 18 Hz. Therefore, $\lambda_{1,2}$ can be confirmed as the SSR mode. The supersynchronous mode will have a frequency of about 99 Hz, which is close to the frequency range of $\lambda_{3,4}$. Hence, it can be confirmed that $\lambda_{3,4}$ represent the supersynchronous mode.

Another confirmation of Mode 1 as the SSR mode comes from Table II. It can be found that the frequency in the SSR mode decreases with the compensation level increasing. For the SSR mode, the higher the compensation level, the higher its frequency. Observed from the synchronous reference frame, then the frequency of the SSR mode is reducing. Meanwhile, the damping ratio of the SSR mode should decrease with an increasing compensation level due to induction generator effect.

The damping of the SSR mode increases when the wind speed increase. This phenomenon can be explained by induction generator effect. A general expression of the stator current can be given as:

$$i_a = \underbrace{\sqrt{2}A\sin(\omega_e t)}_{i_{s1}} + \underbrace{e^{-\alpha t}B\sin(\omega_n t+\theta)}_{i_{s2}} \tag{10}$$

where i_{s1} is the component with a frequency of ω_e which is the frequency of the driving voltages of all the generators and i_{s2} is component with the SSR frequency ω_n.

Consider only i_{s2}, the current component due to LC resonance, the steady-state circuit of the induction generator and the transmission network can be expressed as:

In Fig. 2, the slip s_1 should have the following relationship with the rotating speed f_m and the network resonance frequency f_n:

$$s_1 = \frac{f_n - f_m}{f_n}. \tag{11}$$

$$s_1 \begin{cases} \geq 0 & \text{if } f_n \geq f_m \\ < 0 & \text{if } f_n < f_m \end{cases} \tag{12}$$

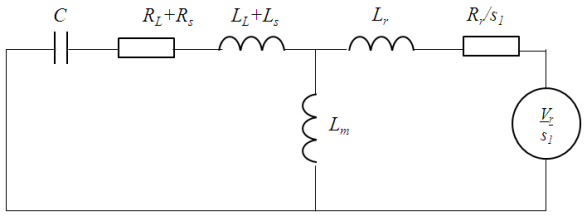

Fig. 2. The equivalent circuit under subsynchronous frequency.

With the wind speed increasing, the corresponding rotating speed f_m increases. The frequency of the network resonance at 75% compensation level f_n is less than any rotating speed f_m. Hence s_1 is a negative number and its absolute value increases when the wind speed increases. In turn, the absolute value of R_r/s_1 decreases. In turn the circuit has less negative resistance and the damping of the SSR mode increases when the wind speed increases.

B. Identification of shaft mode

Participation factor analysis in Table. IV shows that the dominant states for $\lambda_{7,8}$ are the rotating masses' speeds and the torque between the two masses of the wind turbine. Hence it can be concluded that $\lambda_{7,8}$ are related to the shaft mode. The shaft mode is closely related to the mechanical torque, the electromagnetic torque and the rotating speed. Hence wind speed has great impact on the mode. When the wind speed is at 10 m/s, this mode has a negative damping.

C. Identification of electromechanical mode

Observing Table III found that the frequency of $\lambda_{5,6}$ changes along with the wind speed. As mentioned, different wind speed corresponds to different rotating shaft speed. At 7m/s, the speed is 0.75 pu or 45 Hz. At 8m/s, the speed is 0.85 pu or 51 Hz. At 9m/s and 10m/s, the rotating speeds are 57 and 63 Hz respectively. Observation tells that the frequency of the mode is the complimentary of the rotating speed ($60-f_m$). Thus this mode is conjectured to be related to the mechanical dynamics. Further experiments will be performed to better identify this mode.

The rotor resistance R_r is varied. The purpose is to observe if such change has any impact on Mode 3. When the rotor resistance R_r changes (from 0.00549 to 0.1), the eigenvalue loci

of the SSR, super synchronous resonance, electromechanical and shaft mode at 7m/s wind speed and 75% compensation level are shown in the Fig. 3. The shaft mode and the supersynchronous mode are kept relatively constant.Two most notable phenomena are remarked here:

- Increase of R_r leads to an increased damping of Mode 3;
- Increase of R_r leads to a decreased damping of Mode 1 - the SSR mode.

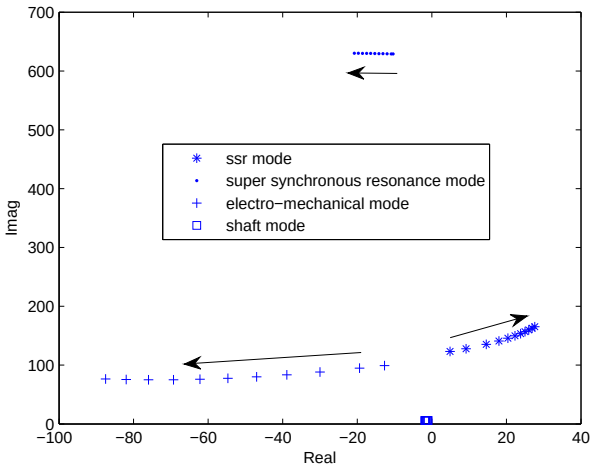

Fig. 3. Eigenvalue loci of the SSR, super synchronous resonance, electromechanical and shaft mode at 7 m/s wind speed and 75% compensation level for increasing rotor resistance($R_r = 0.00549$ to 0.1).

The decrease of damping in the SSR mode can be explained by the induction generator effect (IGE) using the circuit in Fig. 2. At 75% compensation level and 7m/s wind speed, f_n is less than f_m and s_1 is a negative number. Hence for the SSR mode, when R_r increases, the absolute value of R_r/s_1 will be close to and then exceed the sum of the armature and network resistance which lead to negative damping of the circuit or IGE. Therefore, when the rotor resistance R_r increases, the damping of the SSR mode will decrease and the SSR mode will move towards the right half plane. The root loci in Fig. 3 corroborate with the above analysis on the SSR mode.

In the rotor circuits, there is a dc component which is decaying and related to the RL circuit. This component if seen from the rotor circuit has a frequency of 0 HZ. When this dc component is seen from the synchronous reference frame, the frequency of this component will become $f_e - f_m$. Detail expressions of the rotor currents for short circuit transients can be found in [18]. Changing R_r will increase the speed of decaying of this dc component. If the component is seen in the synchronous reference frame, then its damping is increased. Therefore, Mode 3 is related to the rotor circuit dynamics.

The relationship of Mode 3 and the mechanical dynamics however has not been studied in literature. In the following paragraph, the relationship will be explained. The rotor speed dynamics equation give by:

$$2H_g \frac{d\omega_m}{dt} = T_m - T_e \tag{13}$$

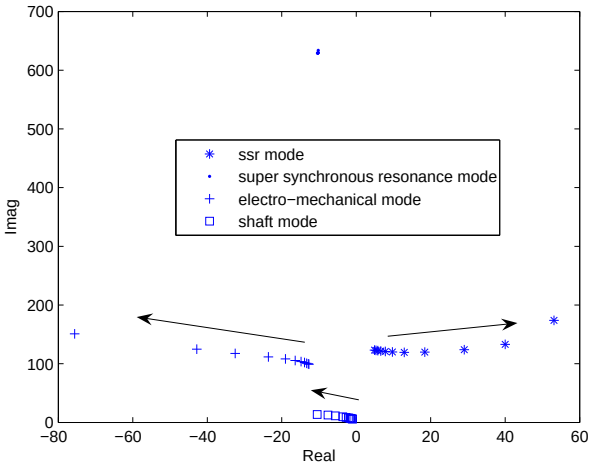

Fig. 4. Eigenvalue loci of the SSR, super synchronous resonance, electromechanical and shaft mode at 7 m/s wind speed and 75% compensation level for a decreasing generator inertia constant($H_g = 0.9$ to 0.01).

where ω_m is the rotor speed, T_m is the mechanical torque and T_e is the electromagnetic torque and $T_e = i_{qs}i_{dr} - i_{ds}i_{qr}$ where i_{qs} and i_{ds} are the quadrature and direct stator currents and i_{qr} and i_{dr} are the quadrature and direct rotor currents.

From (13), it can be found that the components in rotor currents i_{qr} and i_{dr} corresponding to Mode 3 lead to the component in T_e corresponding to Mode 3 and in turn that in ω_m. Further, the dynamics of the rotor speed impact Mode 3. This phenomenon can be observed from Table I: when the wind speed changes, the rotating speed changes and Mode 3 has changes in both frequency and damping. Changing the inertia constant H_g can also have a significant impact on Mode 3 as shown in Fig. 4.

Therefore, Mode 3 is related to both electrical and mechanical dynamics and is called the electromechanical mode.

V. Time Domain Responses - Prediction and Confirmation

Dynamic responses for state variables are impacted by the dominating system modes and their time response coefficients in those state variables. From Section III, it is known that the time response coefficients in time-domain responses are determined by the eigenvector matrices and the initial conditions. In this study, the different initial conditions are due to the change of the wind speeds and the compensation levels. This section gives the computation results of the time response coefficients from modal analysis, which will be used to analyze and quantify the nonlinear time-domain simulation results.

For different wind speeds (from 7 m/s to 10m/s) and different compensation level, the time response coefficients can be computed according to Section III. Tables V-VIII list the time response coefficients corresponding to each mode for each state variable. Figs. 5-8 show the nonlinear time-domain simulation results of stator current (i_{qs}, i_{ds}), rotor current (i_{qr}, i_{dr}), line current (i_{qe}, i_{de}), capacitor voltage (v_{cq}, i_{cd}), electrical torque (T_e) and rotor speed (ω_m) under different wind speeds (from 7 m/s to 10m/s) with 75% compensation

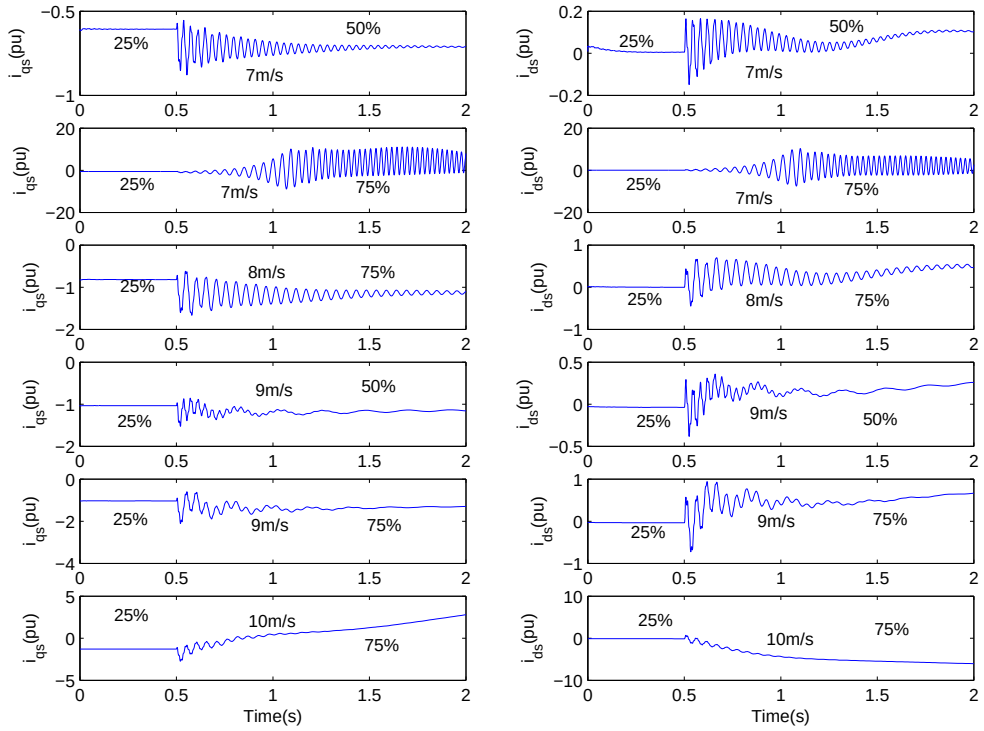

Fig. 5. Simulation results of i_{qs} and i_{ds} under different wind speeds and different compensation levels. At initial condition, the compensation level is 25%.

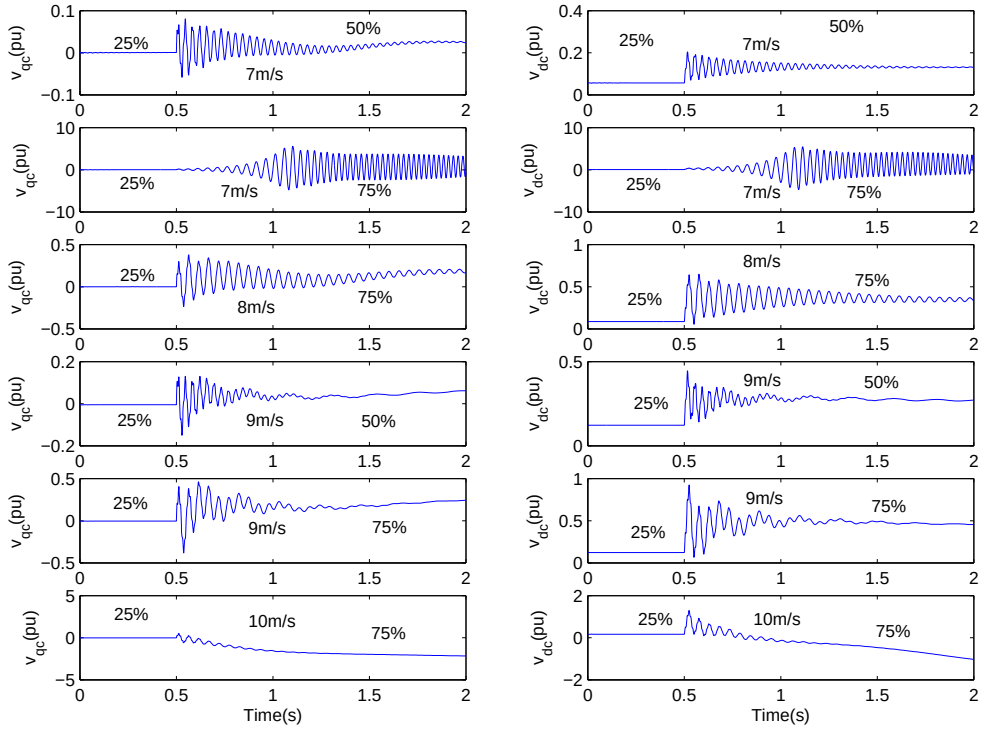

Fig. 6. Simulation results of v_{cq} and v_{cd} under different wind speedsand different compensation levels. At initial condition, the compensation level is 25%.

TABLE V
TIME RESPONSE COEFFICIENTS AT 7M/S WIND SPEED WITH 75% COMPENSATION LEVEL

State Variable	SSR mode 4.9+j123.2	EM mode -12.7+j99	Shaft mode -1+j5.8
q−axis stator current i_{qs}	1075	1631	22
d−axis stator current i_{ds}	1061	1477	111
q−axis rotor current i_{qr}	1054	1652	23
d−axis rotor current i_{dr}	1040	1495	121
q−axis line current i_{qe}	-1005	1394	21
d−axis line current i_{de}	992	1407	110
turbine speed ω_t	0.005	0.011	2.02
machine speed ω_m	3.51	6.32	8.97
Torque in mass 1−2 T_{12}	1.61	3.58	104
q−axis capacitor voltage v_{qc}	554	711	41
d−axis capacitor voltage v_{dc}	557	710	8.16
Electrical Torque T_e	777	1133	23.7

TABLE VI
TIME RESPONSE COEFFICIENTS AT 8M/S WIND SPEED WITH 75% COMPENSATION LEVEL

State Variable	SSR mode -2.1+j121.8	EM mode -5.7+j63.2	Shaft mode -1.5+j5.4
q−axis stator current i_{qs}	316	990	57
d−axis stator current i_{ds}	315	844	232
q−axis rotor current i_{qr}	309	1034	61
d−axis rotor current i_{dr}	308	884	253
q−axis line current i_{qe}	314	818	57.2
d−axis line current i_{de}	307	816	229
turbine speed ω_t	0.0015	0.019	2.77
machine speed ω_m	1.04	6.25	11.2
Torque in mass 1−2 T_{12}	0.48	5.57	137
q−axis capacitor voltage v_{qc}	171	367	86
d−axis capacitor voltage v_{dc}	173	368	21.7
Electrical Torque T_e	225	706	57.6

TABLE VII
TIME RESPONSE COEFFICIENTS AT 9M/S WIND SPEED WITH 75% COMPENSATION LEVEL

State Variable	SSR mode -4.3+j121.4	EM mode -2.5+j30.5	Shaft mode -1.4+j2.8
q−axis stator current i_{qs}	69	494	260
d−axis stator current i_{ds}	61	354	627
q−axis rotor current i_{qr}	60	531	279
d−axis rotor current i_{dr}	60	376	684
q−axis line current i_{qe}	64	458	254
d−axis line current i_{de}	62	320	607.5
turbine speed ω_t	0.003	0.05	9.87
machine speed ω_m	0.201	6.72	10.5
Torque in mass 1−2 T_{12}	0.09	12.51	265.7
q−axis capacitor voltage v_{qc}	34	135	228
d−axis capacitor voltage v_{dc}	35	182	95.5
Electrical Torque T_e	43	355	231.6

TABLE VIII
TIME RESPONSE COEFFICIENTS AT 10M/S WIND SPEED WITH 75% COMPENSATION LEVEL

State Variable	ssr mode -5.4+j120.7	EM mode -5.9+j27.8	shaft mode 0.5+j4.4
q−axis stator current i_{qs}	53	325	51
d−axis stator current i_{ds}	55	199	250
q−axis rotor current i_{qr}	52	359	57
d−axis rotor current i_{dr}	53	219	272
q−axis line current i_{qe}	59	363	55
d−axis line current i_{de}	56	210	249
turbine speed ω_t	0.0002	0.045	1.95
machine speed ω_m	0.18	4.88	381
Torque in mass 1−2 T_{12}	0.08	9.8	72
q−axis capacitor voltage v_{qc}	31	70	93
d−axis capacitor voltage v_{dc}	32	130	19
Electrical Torque T_e	38	236	37

level. The dynamics are initiated at $t = 0.5$s when the original compensation level (25%) is changed to 50% or 75%.

Remarks from the observation of Tables V-VIII are listed as:

1) Dominating systems modes are changing with changing operating conditions. For example, at 7m/s and 8m/s wind speed, the dominating mode is the SSR mode alone. The electromechanical mode and the shaft mode have enough damping. When the wind speed is 9 m/s, the dominating modes are the electromechanical mode and the SSR mode. When the wind speed is 10 m/s, the dominating modes are the shaft mode and the SSR mode.
2) When the speed is low (7m/s and 8m/s) the SSR mode is most obvious in the voltages and currents as the corresponding time response coefficients are relatively large. It is not obvious in the torques and speeds.
3) When the wind speed is high, the shaft mode is most obvious in the torques and speeds as the corresponding time response coefficients are large. It is not obvious in electrical variables such as voltages and currents.
4) When the speed is high (9m/s and 10m/s) the electromechanical mode and the shaft mode are dominant in the time-domain responses of the voltages and currents. The SSR mode is no longer dominant. The SSR mode also has a better damping when the wind speed is high.
5) The electromechanical mode can be observed in the electromagnetic torque, the generator speed, and the voltages and currents.

For example, the simulation results of i_{qs} at 8m/s with 75% compensation level and at 9m/s at 50% or 75% show that when the wind speed is low (8m/s), it is the SSR mode dominating the dynamic response; but when the wind speed is high (9m/s), it is the electromechanical mode dominating the dynamic responses since the SSR mode can be damped out fast. At the same operating condition, the shaft mode is more obvious in d-axis currents than in q-axis from Fig. 5. For the series capacitor voltages, the shaft mode is more obvious in the q-axis variable (Fig. 6). From the time response coefficients tables, the coefficients of the shaft mode in d-axis currents are much greater than that in q-axis currents. This explains the difference in nonlinear simulation results.

Fig. 7 shows the dynamic responses of the electromagnetic torque T_e at different wind speeds and different compensation levels. The dynamic responses confirm remark (1).

The dynamic responses of the rotor speed are shown in Fig. 8. From the time response coefficient table, the response of rotating speed ω_m is determined largely by the electromechanical mode and the shaft mode at all wind speeds and compensation levels. Therefore, the electric network resonance mode or the SSR mode is not obvious in the rotor speed responses.

Study of time response coefficients has potential applications. One example is that it can help choose suitable feedback signals when SSR mitigation is of concern. In conventional synchronous generator systems, torsional interaction is a big concern in SSR phenomena. Unlike such systems, in wind energy systems, due to the low shaft stiffness, the shaft mode has a very low frequency and torsional interaction rarely

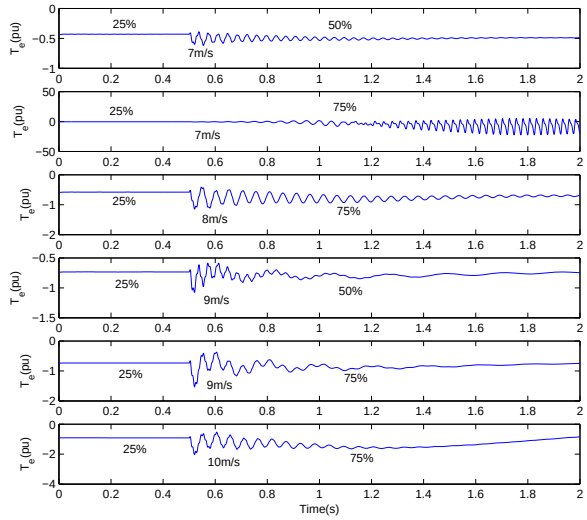

Fig. 7. Simulation results of Te under different wind speeds and different compensation levels. At initial condition, the compensation level is 25%.

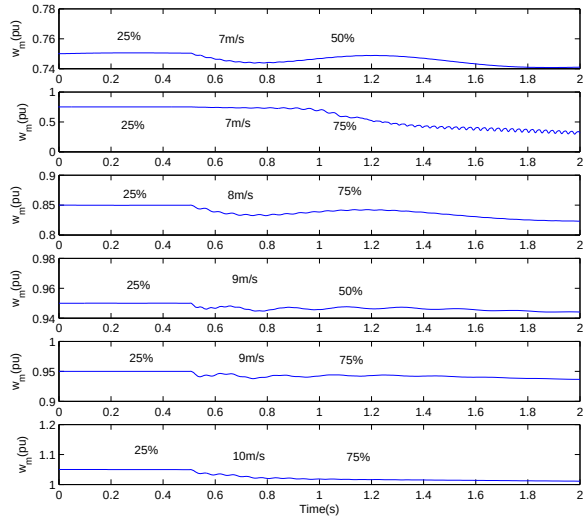

Fig. 8. Simulation results of ω_m under different compensation levels and different compensation levels. At initial condition, the compensation level is 25%.

happens. Rotor speed or frequency has been used as the feedback signal for SSR mitigation in conventional power systems via FACTS devices [19] and in wind energy systems [2], [4]. Our study shows that for wind energy systems, rotor speed does not reflect the network resonance mode well. Hence in such systems, a better choice should be made. Such inquiry was made in a recent submitted paper [20].

VI. Conclusion

Modal analysis is performed for a DFIG-based wind energy system interconnected with a series-compensated electric network. Four system modes are identified, namely, the SSR mode, the super-synchronous resonance mode, the electromechanical mode and the shaft mode using eigenvalue analysis and participation factor. Parameters and operating conditions are varied to confirm the characteristics of those system modes and demonstrate their impact on those system modes. Unique findings documented in this paper include (i) the nature of the electromechanical mode and its relation with the wind speed; (ii) the relationship between the shaft mode and the wind speed, and (iii) time response coefficients computed based on modal analysis in order to predict the dynamic performance of different variables. The predictions are confirmed by nonlinear time-domain simulation results.

Appendix

TABLE IX
PARAMETERS OF A SINGLE 2 MW DFIG AND THE AGGREGATED DFIG IN NETWORK SYSTEM

Rated power	2 MW	100 MW
Rated voltage	690 V	690 V
X_{ls}	0.09231 pu	0.09231 pu
X_M	3.95279 pu	3.95279 pu
X_{lr}	0.09955 pu	0.09955 pu
R_s	0.00488 pu	0.00488 pu
$R_r^{'}$	0.00549 pu	0.00549 pu
H	3.5 s	3.5 s
X_{tg}	0.3 pu (0.189 mH)	0.3 pu ($\frac{0.189}{5}$ mH)
DC link capacitor C	$14000\mu F$	$50 \times 14000\mu F$
DC link rated voltage	1200 V	1200 V

TABLE X
PARAMETERS OF THE NETWORK SYSTEM

Transformer ratio	690V/161 kV
Base MVA	100 MVA
R_L	0.02 pu (5.1842Ω)
X_L	0.5 pu (129.605Ω)
X_C at 50% compensation level	64.8Ω
Series compensation C	40μF
Line length	154 mile

TABLE XI
PARAMETERS OF THE SHAFT SYSTEM

H_1	0.9 s
H_2	4.29 s
D_1	0 pu
D_2	0 pu
D_{12}	1.5 pu
K_{12}	0.15 pu

Acknowledgement

The authors would like to acknowledge NSF for its support through EECS-0901213. This paper is partly supported by China Scholarship Council.

References

[1] IEEE Committee Report, "Terms, definitions, and symbols for subsynchronous resonance oscillations," *IEEE Trans. Power App. Syst.*, vol. 104, pp. 1326–1334, Jun. 1985.

[2] R. Varma, S. Auddy, and Y. Semsedini, "Mitigation of subsynchronous resonance in a series compensated wind farm using FACTS controllers," *IEEE Trans. Power Del.*, vol. 23, no. 3, pp. 1645–1654, Jul. 2008.

[3] A. Ostadi, A. Yazdani, and R. Varma, "Modeling and stability analysis of a DFIG-based wind-power generator interfaced with a series-compensated line," *IEEE Trans. Power Del.*, vol. 24, no. 3, pp. 1504–1514, Jul. 2009.

[4] M. S. El-Moursi, B. Bak-Jensen, and M. H. Abdel-Rahman, "Novel STATCOM controller for mitigating SSR and damping power system oscillations in a series compensated wind park," *IEEE Trans. Power Electron.*, vol. 25, no. 2, pp. 429–441, Feb. 2010.

[5] F. Mei and B. Pal, "Modal analysis of grid-connected doubly fed induction generators," *IEEE Trans. Energy Convers.*, vol. 22, no. 3, pp. 728–736, Sep. 2007.

[6] F. Mei and B. C. Pal, "Modelling of dobuly-fed induction generator for power system stability study," *Proceedings of IEEE Power & Energy General Meeting 2008*, Jul. 2008.

[7] IEEE Committee Report, "First benchmark model for computer simulation of subsynchronous resonance," *IEEE Trans. Power and Apparatus Systems*, vol. 96, no. 5, pp. 1565–1672, Sep./Oct. 1977.

[8] N. W. Miller, W. W. Price, and J. J. Sanchez-Gasca, "Dynamic modeling of ge 1.5 and 3.6 wind turbine-generators," *GE-Power Systems Energy Consulting, General Electric International, Inc., Schenectady, NY*, Oct. 2003.

[9] Z. Miao and L. Fan, "The art of modeling high-order induction generator in wind generation applications," *Simulation Modelling Practice and Theory*, vol. 16, no. 9, pp. 1239–1253, Oct. 2008.

[10] J. Sun, "Small-signal methods for ac distributed power systemsa review," *IEEE Trans. Power Electron.*, vol. 24, no. 11, pp. 2545–2554, Nov. 2009.

[11] C. Zhu, L. Fan, and M. Hu, "Modeling and simulation of a DFIG-based wind turbine for SSR," in *North American Power Symposium (NAPS)*, Mississippi State University, Starkville MS, Oct. 2009.

[12] L. Fan, R. Kavasseri, Z. Miao, and C. Zhu, "Modeling of DFIG-based wind farms for SSR analysis," *under review, IEEE Trans. Power Delivery*.

[13] C. Zhu, L. Fan, and M. Hu, "Modeling and simulation of a DFIG-based wind turbine for SSR," *accepted, IEEE PES General Meeting 2010*.

[14] G. Rogers, *Power System Oscillations*. Kluwer Academic Publishers, 2000.

[15] P. Anderson, B. Agrawal, and J. V. Ness, *Subsynchronous Resonance in Power Systems*. IEEE Press, 1990.

[16] P. Kundur, *Power System Sability and Control*. McGraw Hill, 1994.

[17] S. Joshi and A. Kulkarni, "Analysis of ssr performance of TCSC control schemes using a modular high bandwidth discrete-time dynamic model," *IEEE Trans. Power Syst.*, vol. 24, no. 2, pp. 840–848, May 2009.

[18] D. D. Li, "Analysis and calculation of short circuit current of doubly fed induction generator," in *IEEE PES Transmission and Distribution Conference and Exposition*, Chicago, IL, Apr. 2008.

[19] N. Hingorani and L. Gyugyi, *Understanding FACTSConcepts and Technology of Flexible AC Transmission System*. New York: IEEE Press, 2000.

[20] L. Fan and Z. Miao, "Mitigating SSR using DFIG-based wind generation," *submitted to IEEE Trans. Power Delivery*.